Simulation of physical processes

GENERALIZED CORRECTION TO EMBEDDED-ATOM POTENTIALS FOR SIMULATION OF EQUILIBRIUM AND NONEQUILIBRIUM PROPERTIES OF METALS

**A.V. Verkhovtsev[1], A.V. Korol[1], G.B. Sushko[1],
S. Schramm [2], A.V. Solov'yov[1]**

[1] MBN Research Center at Frankfurt Innovation Center of Biotechnology,
Frankfurt am Main, Germany;

[2] Goethe University Frankfurt, Frankfurt am Main, Germany

A modification of an embedded-atom method (EAM)-type potential is proposed for a quantitative description of equilibrium and nonequilibrium properties of metal systems within the molecular dynamics framework. The modification generalizes the previously developed linear correction to EAM-type potentials [Sushko et al., J. Phys.: Condens. Matter 28 (2016) 145201] and asymptotically approaches zero at large interatomic distances. A general procedure for constructing this modification is outlined and its relation to the linear correction is elaborated. To benchmark this procedure, we examine the melting phase transition and several equilibrium properties of finite-size nanosystems made of silver, gold and titanium. The simulations performed with the modified potential predict higher bulk melting temperatures of the metals and agree better with experimental values as compared to the original EAM-type potential. Our results show that the modification works well for metals with both cubic and hexagonal lattice structures. The Gupta potential is chosen as an example but the modification proposed can also be applied to other potentials of the EAM type.

Keywords: molecular dynamics simulation, many-body potential, phase transition, equilibrium properties, metal nanoparticle

ОБОБЩЕННАЯ ПОПРАВКА К ПОТЕНЦИАЛАМ ПОГРУЖЕННОГО АТОМА ДЛЯ МОДЕЛИРОВАНИЯ РАВНОВЕСНЫХ И НЕРАВНОВЕСНЫХ СВОЙСТВ МЕТАЛЛОВ

**А.В. Верховцев[1], А.В. Король[1], Г.Б. Сушко[1],
Ш. Шрамм [2], А.В. Соловьёв[1]**

[1] Научно-исследовательский центр мезобионаносистем,
г. Франкфурт-на-Майне, Германия;

[2] Университет им. Гёте, г. Франкфурт-на-Майне, Германия

Предложена модификация потенциалов погруженного атома (EAM) для описания равновесных и неравновесных свойств металлических систем в рамках классической молекулярной динамики. Данная модификация обобщает разработанную ранее авторами линейную поправку к потенциалам типа EAM и асимптотически убывает на больших межатомных расстояниях. Описана процедура построения модифицированных потенциалов и показана связь данной модификации с линейной поправкой. Предложенная модификация использована для моделирования процесса плавления и изучения ряда равновесных свойств наносистем из серебра, золо-

та и титана. Результаты расчетов, проведенных при помощи модифицированного потенциала, предсказывают более высокие температуры плавления металлов, по сравнению с изначальным потенциалом типа EAM, что лучше согласуется с экспериментальными данными. Многочастичный потенциал типа Гупта рассмотрен в качестве примера, но предложенная модификация может также применяться и к другим потенциалам типа EAM.

Ключевые слова: метод молекулярной динамики, многочастичный потенциал, фазовый переход, металлическая наночастица

Introduction

Computer simulations based on atomistic models have emerged as a powerful tool for the analysis of physicochemical processes occurring in materials and related materials properties [1]. A vast number of atomistic simulations employ molecular dynamics (MD) methods that require the evaluation of total potential energy of many-atom systems and the forces acting on constituent atoms [2, 3]. MD simulations provide insights into many physical processes, such as diffusion [4 − 6], plastic deformation [7, 8], melting [9 − 11], crystallization [10, 12] and other phase transformations [13, 14]. All of these processes happen on temporal and spatial scales exceeding by far those accessible by *ab initio* methods. In order to reach these scales, semi-empirical interatomic potentials parameterized for specific material compositions and structures are used [3, 15 − 17]. A potential constructed by fitting to a specific set of properties should perform well for other properties that were not explicitly considered during its construction phase [18].

Different interatomic potentials [19 − 24] belonging to a general class of embedded-atom method (EAM)-type potentials are commonly used in MD simulations of metal systems [25]. In the past decades, more complex potentials, based on the modified EAM (MEAM) or the second-neighbor (2NN) MEAM, have also been developed for different metals and alloys (see, e.g., a few recent examples [26, 27]). Parameters of these potentials are usually fitted to reproduce experimental data on the properties of bulk materials (e.g., cohesive energy, equilibrium lattice constants, bulk modulus, elastic constants, vacancy-formation energy, etc.) or fitted to zero-temperature *ab initio* calculations of perfect crystalline structures.

It has also been widely discussed that EAM-type potentials are less accurate in describing the dynamics of systems being far from equilibrium, for instance, the melting phase transition. In particular, these potentials often struggle to reproduce the experimental values of melting temperature for bulk metals and yield the discrepancy up to several hundred degrees [5, 28 − 30]. This indicates the necessity to modify the exploited force fields in order to enable a more accurate description of systems' properties at elevated temperatures. An accurate description of both equilibrium and nonequilibrium properties of metal systems is important, e.g., for studying irradiation-driven phase and structural transformations of nanostructures [31, 32] or irradiation-induced chemistry underlying novel nanofabrication techniques [33, 34].

Different approaches to account for finite-temperature effects in classical force fields for metal systems have been discussed in literature. A method for re-parameterization of interaction potentials was proposed [35] to adjust the calculated melting temperature of materials without affecting mechanical properties to which the potentials were fitted. In that method, the melting temperature was calculated using a trial interatomic potential and the Gibbs − Duhem equation (which relates changes in the chemical potential of a system to changes in its temperature and pressure) was then solved to update the

parameters of potentials. This method was applied [35] to re-parameterize an EAM-type potential for Al and improved the calculated bulk melting temperature without considerable change in other properties. A correction to a many-body force field for titanium proposed in Ref. [36] included the contribution of thermal excitations of electronic degrees of freedom. In that approach, an EAM-type potential was augmented by an additional term (related to electronic entropy) that arises from the Sommerfeld theory of metals. According to that theory, there is a temperature-dependent contribution to the free energy of a metal system that depends also on the density of states at the Fermi energy. In Ref. [37], several parameterizations of EAM-type potentials for Ti describing defects, plasticity and melting were presented. These potentials fit well to either low- or high-temperature experimental data but could not describe both temperature regions simultaneously. On this basis, a temperature-dependent potential, being a combination of potentials operating better in different regions, was suggested to study the properties of Ti in a wide temperature range. The knowledge accumulated in these studies suggests that modifications of conventional EAM-type potentials are required in order to match the calculated nonequilibrium properties (the melting temperature in particular) of metal materials to experimental values.

In our previous work [38], we presented a modification of an EAM-type potential (considering a many-body Gupta potential [39] as an example). With that modification, both the melting temperature and the near-equilibrium properties of selected metal systems were reproduced. It was revealed that augmenting steepness of the interaction potential by enhancing its repulsive part leads to an increase of the melting temperature. This happens because a higher thermal energy is needed to reach the threshold of atomic vibration amplitudes at which the melting occurs. To that end, the original EAM-type potential was augmented by adding a linear term to the repulsive part [38]. The linear correction represented a minor change to the potential energy but led to a significant increase of the melting temperature. It was applied to study thermal, geometrical and energetic properties of magnesium, titanium, platinum and gold, yielding a good agreement with experimental results. In Ref. [40], this method was used to evaluate melting points of finite-size NiTi nanoalloys with different composition of Ni and Ti. These results were used to evaluate bulk melting temperatures of $Ni_{1-x}Ti_x$ alloys, which agreed with an experimental phase diagram for the NiTi material.

In this paper, the previously developed methodology is generalized in the form of a new modification of an EAM-type potential. This modification represents a linear function multiplied by a sigmoid function, which gradually tends to zero beyond a given distance. A general procedure for constructing this modification is outlined and its parameters are related to the parameters of the linear correction [38]. The modified EAM-type potential is used for MD simulations of melting of nanometer-sized nanoparticles made of silver, gold and titanium. Structural and energetic equilibrium properties of these systems, such as lattice constants, cohesive energy and vacancy formation energy are also analyzed. Our results demonstrate that the new modification is applicable for metals with both cubic and hexagonal crystalline lattices. To be consistent with our previous works [38, 40] the Gupta potential is considered as an example but we stress that the modification proposed can also be applied to other interatomic potentials of the EAM type, e.g., to Sutton – Chen [20] or Finnis – Sinclair [41] potentials.

EAM-type Gupta potential

Similar to other many-body potentials of the EAM type, the Gupta potential is constructed as a sum of (*i*) a short-range repulsive term that stems from the repulsion between atomic cores and (*ii*) a long-range attractive term which imitates delocalization of the outer-shell electrons and is related to electron density at a given atomic site. The total energy of an *N*-atom system interacting via an EAM-type potential reads as

$$U = \frac{1}{2}\sum_{i=1}^{N}\sum_{j\neq i} V(r_{ij}) + \sum_{i=1}^{N} F_i(\rho_i), \qquad (1)$$

where $V(r_{ij})$ is the short-range repulsive interaction between atoms i and j separated by the distance r_{ij}; the attractive term F_i stands for the energy obtained by embedding atom i into the local electron density ρ_i provided by the remaining atoms of the system.

The functional form of $F_i(\rho_i)$ may vary in different EAM-type potentials [25] while the Gupta potential employs a specific form of this function,

$$F_i(\rho_i) \propto -\sqrt{\rho_i}.$$

This functional form is based upon the second-moment approximation of the tight-binding model [42, 43], according to which the attractive many-body term is related to the energy of d valence electron band and expressed as a square root of ρ_i. The latter is constructed empirically as a linear superposition of electron charge densities of constituent atoms,

$$\rho_i = \sum_{j \neq i} \psi(r_{ij}).$$

Within the Gupta representation, the functions $V(r_{ij})$ and $\psi(r_{ij})$ are introduced in exponential forms so that the total potential energy U_{Gup} reads as follows:

$$U_{Gup} = \sum_{i=1}^{N} \left[\frac{1}{2} \sum_{j \neq i} A e^{-p\left(\frac{r_{ij}}{d}-1\right)} - \sqrt{\sum_{j \neq i} \xi^2 e^{-2q\left(\frac{r_{ij}}{d}-1\right)}} \right], \tag{2}$$

where d is the first-neighbor distance; p, q are related to bulk elastic constants; ξ represents an effective orbital-overlap integral; A adjusts the cohesive energy.

The parameters for silver, gold and titanium used in this work were taken from Ref. [22].

Linear correction to EAM-type potentials

The EAM-type Gupta potential (2) corrected with the linear term U_{lin} introduced in Ref. [38] reads

$$U = U_{Gup} + U_{lin} \equiv$$
$$\equiv U_{Gup} + \frac{1}{2} \sum_{i,j=1}^{N} \left(B r_{ij} + C \right), \tag{3}$$

where B and C are parameters.

The linear form was chosen to match the curvature of the modified potential energy profile in the vicinity of the equilibrium point (governed by the second derivative of potential energy U) to that of the original EAM-type potential.

As discussed in Ref. [38], the term $B r_{ij}$ ($B > 0$) makes the potential energy profile steeper at interatomic distances exceeding the equilibrium point r_0 whilst also slightly changing the depth of the potential well at r_0. The constant term $C < 0$ was therefore added to mitigate the latter effect. In Ref. [38], parameters B and C were obtained empirically for a specific cutoff distance r_c for titanium, gold, platinum and magnesium. As shown below, these parameters can be derived for any material and any r_c using the following analytical estimate.

The correction to an EAM-type potential should not change the cohesive energy of a bulk material to which the potential was fitted. Therefore, the change in the total potential energy due to a linear correction should be equal to zero. If we approximate the real crystalline structure of a metal with a uniform distribution of atoms with number density n_0, this condition can be written as

$$\int_{r < r_c} n_0 \left(B r_{ij} + C \right) dV = 0, \tag{4}$$

leading to the relation

$$C = -\frac{3}{4} B r_c. \tag{5}$$

Fig. 1 shows (by lines) the calculated dependence $C(B)$ for gold and titanium for different values of r_c. These parameters of the linear correction leave intact the cohesive energy of bulk metal systems. Bulk gold and silver have fcc crystal lattices and very similar lattice constants, so the results shown for gold also describe silver crystals. For each metal we consider three cutoff distanc-

es between 6 and 8 Å, corresponding to minima in the radial distribution function (see the vertical lines in Fig. 2). The indicated values of r_c were chosen following Ref. [22]. In that work, the parameters of the Gupta potential for the fcc metals were derived accounting for interatomic interactions up to the fifth-neighbor shell, while the suggested cutoff values for titanium and other hcp structures corresponded to inclusion of seven to eight shells of neighboring atoms.

The linear correction causes a small displacement Δr of atoms from their equilibrium positions defined by the original EAM-type potential. Expanding U in a Taylor series about the equilibrium atomic positions for the original potential and keeping only the first term of this expansion one evaluates a change in potential energy associated with Δr as

$$\Delta U = -F_{lin}\Delta r =$$
$$= -\frac{2\pi}{3}\left(\frac{4}{3}\right)^3\frac{C^3}{B^2}n_0\Delta r. \tag{6}$$

As it was demonstrated in our earlier work [38], augmenting steepness of the interatomic potential beyond the equilibrium point by enhancing the repulsive contribution of the force field leads to a rise of the melting point. It happens because an increased thermal energy is needed to reach the threshold of atomic vibration amplitudes at which the melting phase transition occurs. Knowing the experimental bulk melting temperature T_m^{exp} and the value predicted by the original Gupta potential, T_m^{Gup}, parameters B and C can be chosen such that an increase in the melting temperature will be equal to $\Delta T = T_m^{exp} - T_m^{Gup}$.
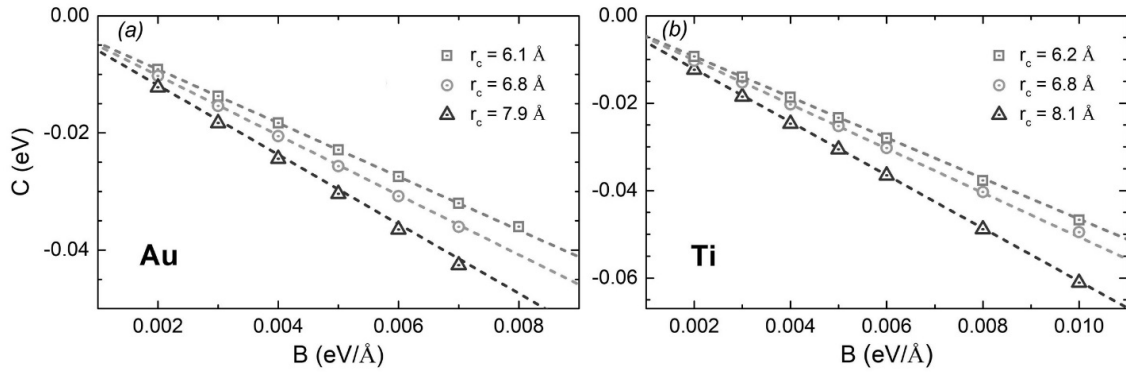

Fig. 1. The $C(B)$ dependence for Au (*a*) and Ti (*b*) for different cutoff values r_c; lines show the results obtained using Eq. (5); symbols show the results of structure optimization calculations which account for the realistic crystal structures (see the 'Results and discussion' section)
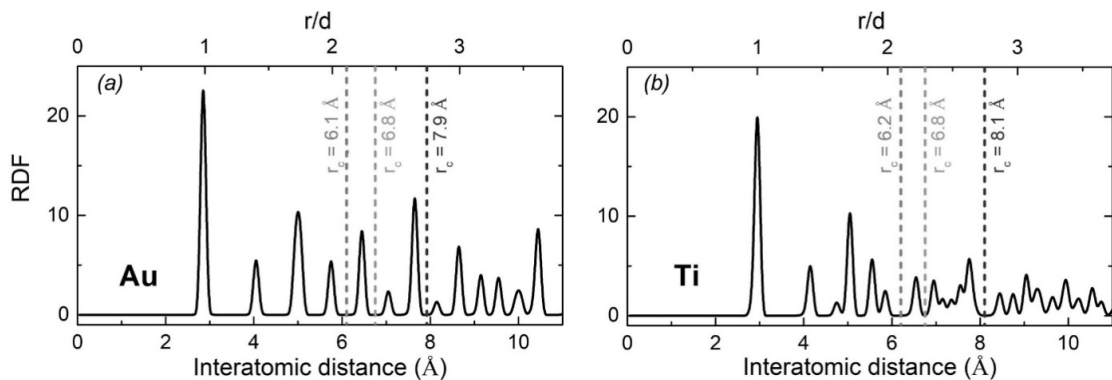

Fig. 2. The calculated radial distribution functions (RDFs) for 10-nm Au (*a*) and Ti (*b*) nanoparticles (composed of approximately 30,000 atoms). The used cutoff values r_c are shown by dashed lines

Eqs. (5) and (6) define, for any r_c, a combination of parameters B, C that reproduce experimental values of cohesive energy and melting temperature of bulk materials. These conditions were used to define B and C for the three metals studied.

Generalized modification of EAM-type potentials

In this section, we generalize the above described methodology and propose a new modification of an EAM-type potential. The modification should keep features of the linear correction, i.e., maintain its behavior in the vicinity of atomic equilibrium points and enhance the repulsive interactions with an increase of atomic displacements. We construct the modification in such a way that it contains a parameter describing the characteristic range of the potential thus eliminating the dependence of the potential on the choice of the cutoff distance. These conditions are fulfilled by multiplying U_{lin} by a sigmoid function which is equal to unity at small interatomic distances and asymptotically approaches zero beyond a given distance. The modified EAM-type Gupta potential then reads as

$$U = U_{\text{Gup}} + U_{mod} \equiv$$
$$\equiv U_{\text{Gup}} + \frac{1}{2} \sum_{i,j=1}^{N} \frac{\tilde{B} r_{ij} + \tilde{C}}{1 + e^{\lambda(r_{ij} - r_s)}}. \quad (7)$$

The parameters $\tilde{B}$ and $\tilde{C}$ have the same meaning as B and C in Eq. (3): $\tilde{B}$ defines an additional force acting on the nearest atoms and $\tilde{C}$ adjusts the depth of the potential well in the vicinity of the equilibrium point where $U = 0$. The parameter λ describes the slope of U_{mod} at large interatomic distances, while r_s defines the sigmoid's midpoint and hence the range of this potential. Fig. 3 shows the potential U_{mod} for a pair of atoms as a function of interatomic distance r. Due to its sigmoid-type shape, $U_{mod}(r)$ asymptotically approaches zero and its range serves as a natural cutoff distance for this interaction.

For each pair of atoms, the potential U_{lin} grows monotonically with interatomic distance up to the cutoff r_c, and all atoms located within the sphere of radius r_c experience the same force exerted by a given atom. On the contrary, U_{mod} has a maximum at interatomic distances of about $5 - 8$ Å depending on the choice of λ and r_s (see Fig. 3). Thus, the force exerted by an atom due to U_{mod}
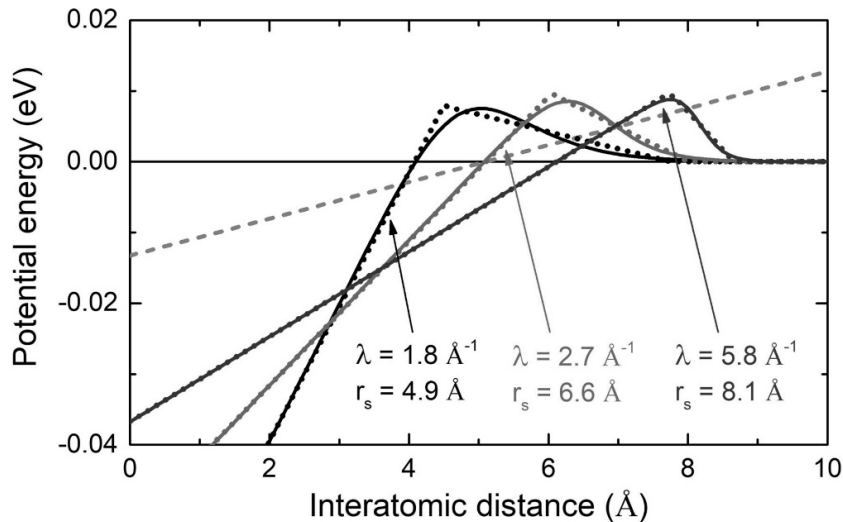

Fig. 3. Plots of $U_{mod}(r)$ (7) for different values of the parameters (solid lines) and U_{lin} (a dashed gray line) vs. the interatomic distance r, and also the piecewise linear approximation $\bar{U}_{mod}(r)$ (8) (dotted curves, see the Appendix for details). The used procedure of deriving the parameter values is given in the text

enhances interaction with several nearest atomic shells while the interaction with more distant atoms weakens. The strength of this interaction is governed by the steepness of the potential beyond its maximum, i.e., by the parameter λ. Therefore, the force acting on the nearest neighbors due to U_{mod} should exceed (by the absolute value) the force F_{lin} as its effect is compensated by weaker interactions with more distant atoms. Thus, for each pair of atoms interacting via $U_{mod}(r)$, the initial slope of the potential should be steeper than the slope of $U_{lin}(r)$, i.e. $\tilde{B} > B$.

To analytically derive parameters of the new modification, $U_{lin}(r)$ in Eqs. (4) and (6) was substituted with $\bar{U}_{mod}(r)$ – a piecewise linear approximation of the sigmoid-type function $U_{mod}(r)$, see Eq. (8) in Appendix. Then, parameters of this function were expressed through the parameters B and C of the linear correction. As a last step of this procedure, $\bar{U}_{mod}(r)$ was fitted with $U_{mod}(r)$ to derive λ and r_s. Further technical details are given in the Appendix. The parameters of U_{mod} used for an analysis of melting temperature and near-equilibrium properties of silver, gold and titanium nanosystems are summarized in Table 1. Details of this analysis are presented below in the 'Results and Discussion' section.

The modification U_{mod} (7) is qualitatively similar to the well-known Dzugutov potential [45] which was developed to model glass-forming liquid metals. The Dzugutov potential coincides with the Lennard − Jones potential at small interatomic distances but has a maximum beyond the equilibrium point. This enables the suppression of crystallization and enforces the emergence of icosahedral structures. The maximum of U_{mod} corresponds to the positions of more distant atoms (see Fig. 3 and the RDFs in Fig. 2). As a result, the modification U_{mod} does not affect crystal structure but leads to an increase in the melting temperature whilst slightly changing the near-equilibrium properties of metals.

Computational details

All simulations described in this work were conducted using the MBN Explorer software package [46]. We considered spherical nanoparticles with radii from 1 to 5 nm (ranging from 250 to 30,000 atoms) that were cut from ideal silver, gold and titanium crystals. The systems were constructed using the MBN Studio software [47].

Prior to the analysis of the structural and energetic parameters of each system, energy minimization calculations were performed using the velocity-quenching algorithm. The MD simulations of the melting process were performed using a large simulation box of $20 \times 20 \times 20$ nm in the NVT canonical ensemble. The temperature T was controlled by a Langevin thermostat with a damping time of 1 ps. The nanoparticles were heated up (starting from the initial temperature T_0 well below the expected melting temperatures, $T_0 = 300$ K for Ag and Au and 1000 K for Ti) with a constant heat rate of 0.5 K/ps, which is within the range of typical values used for MD simulations of phase transitions. The total simulation time for each run was 3 ns. The time integration of the equations of motion was done using the velocity-Verlet algorithm [2] with an integration time step of 1 fs. In the calculations performed with the linear correction U_{lin}, the interatomic interactions were truncated at the cutoff radius r_c

T a b l e 1

Parameters of the potential U_{mod}

Element	$\tilde{B}$, eV/Å	$\tilde{C}$, eV	λ, Å^{-1}	r_s, Å
Ag	0.009	− 0.048	5.93	7.10
Au	0.026	− 0.145	4.68	7.36
Ti	0.052	− 0.269	2.77	6.68

N o t a t i o n: $\tilde{B}$ is an additional force acting on the nearest atoms; $\tilde{C}$ adjusts the depth of the potential well in the vicinity of the equilibrium point where $U = 0$; λ describes the slope of U_{mod} at large interatomic distances; r_s defines the sigmoid's midpoint.

ranging from about 6 to 8 Å as shown in Fig. 2. In the case of the potential augmented with U_{mod}, its range served as a natural cutoff distance, which varied between 8 and 9 Å.

The melting temperatures of nanoparticles were determined from the analysis of heat capacity

$$C_V = \left(\partial E / \partial T \right)_V$$

defined as a partial derivative of the internal energy of the system with respect to temperature at a given volume. A sharp maximum of C_V was attributed to the nanoparticle melting and the position of the maximum was referred to as the nanoparticle's melting point. The bulk melting temperature T_m^{bulk} was estimated by extrapolating the obtained values to the $N \to \infty$ limit according to the Pawlow law [48, 49],

$$T_m^{bulk} = T_m + \gamma N^{-1/3}$$

with γ being the factor of proportionality.

Results and discussion

Fig. 1 shows the dependence $C(B)$ that describes the parameters of the linear correction U_{lin} at different values of cutoff r_c. Dashed lines were obtained by means of Eq. (5) within the uniform density model (see the section 'Linear correction to EAM-type potentials'), while symbols show the results of structure optimization of gold and titanium systems with realistic crystal structures. In the case of structure optimization, the parameters B and C were chosen to match experimental cohesive energies [50]. The outcomes of the uniform density model are in good agreement with the results of optimization calculations. Table 2 summarizes the bulk cohesive energy for silver, gold and titanium, calculated with the linear correction as well as the experimental values and the results obtained by means of the original EAM-type Gupta potential.

T a b l e 2

Comparison of the calculated bulk cohesive energy values with experimental data

Element	Bulk cohesive energy, eV per atom			
	U_{Gup}	$U_{Gup} + U_{lin}$	$U_{Gup} + U_{mod}$	Experiment [50]
Ag	2.96	2.96	2.97	2.96
Au	3.78	3.77	3.78	3.78
Ti	4.87	4.87	4.83	4.85

N o t a t i o n: U_{Gup} is the original Gupta potential, Eq. (2); ($U_{Gup} + U_{lin}$) is the one corrected by U_{lin}, Eq. (3); ($U_{Gup} + U_{mod}$) is the one corrected by the sigmoid-type modification U_{mod}, Eq. (7), proposed in this work.
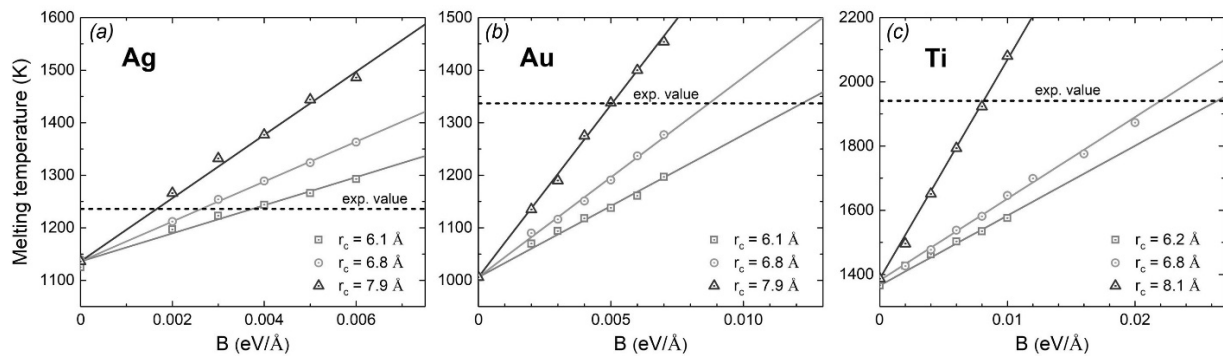

Fig. 4. The calculated dependences of the melting temperature of bulk silver (*a*), gold (*b*) and titanium (*c*) on the parameter B at the different cutoff r_c values (symbols) as well as the least-squares fit to these results (solid lines). Experimental values from Ref. [50] are shown by dashed lines. The calculation procedure is given in the text. $B = 0$ corresponds to the original Gupta potential, Eq. (2)

Fig. 4 shows the melting temperature of bulk silver, gold and titanium calculated using the linear correction U_{lin} to the Gupta potential, Eq. (3), at different values of the parameter B and the cutoff r_c. The parameter C was defined according to Eq. (5). Symbols denote the results of MD simulations of finite-sized nanoparticles melting, extrapolated to the bulk limit. The figure shows that the calculated melting temperature increases linearly with B. These results can be used to evaluate

$$\Delta T = \Delta T_m^{lin}(B) - \Delta T_m^{Gup}.$$

As follows from Eq. (6),

$$\Delta U = k\Delta T \propto \Delta r$$

where Δr stands for an increase in the amplitude of thermal vibrations of atoms with respect to the values predicted by the original Gupta potential.

The slope of $\Delta T(B)$ is therefore proportional to the distance by which the atoms should be additionally displaced from equilibrium positions to initiate the melting process at the temperature corresponding to the experimental value. For silver and gold $\Delta r \approx 0.09$ Å, which is about 3% of their nearest-neighbor distances. For titanium we observed the dependence of Δr on the cutoff distance. For smaller cutoff values, $r_c = 6.2$ Å and 6.8 Å, an increase in the amplitude of thermal vibrations is equal to 0.06 Å and it increases up to 0.09 Å for $r_c = 8.1$ Å. These results suggest that an increase in the amplitude of thermal vibrations by a few percent leads to a dramatic rise of the melting point. A much steeper slope of $\Delta T(B)$ for Ti at $r_c = 8.1$ Å suggests that more distant atoms located in a concentric shell between 7 and 8 Å make a significant contribution to the melting process and the original Gupta potential cannot account properly for this contribution.

Tables 2−4 summarize the results on structural and energetic properties of silver, gold and titanium nanocrystals obtained with the sigmoid-type modification U_{mod} (7). These results are compared to those obtained by means of the original EAM-type Gupta potential (2) and the linear correction U_{lin} (3).

As mentioned above, the calculated bulk cohesive energies are summarized in Table 2. Neither linear correction nor sigmoid-type modification significantly change the values predicted by the original Gupta potential; all these values are in good agreement with experimental data [50] with a relative discrepancy of less than 0.5%.

Table 3 presents the vacancy-formation energy that is the amount of cohesive energy required to form a vacancy in a crystal. It is defined [62, 63] as

$$E_{vf} \equiv (N-1)\left(E_{N-1}^{coh} - E_N^{coh}\right) =$$
$$= E_{N-1} - \frac{N-1}{N}E_N$$

where

$$E_N = NE_N^{coh},$$
$$E_{N-1} = (N-1)E_{N-1}^{coh}$$

are the potential energies of systems containing N and $(N - 1)$ atoms, whereas E_N^{coh} and E_{N-1}^{coh} are the corresponding cohesive energies per atom. The calculated values (columns labeled as 'U_{Gup}', '$U_{Gup} + U_{lin}$' and '$U_{Gup} + U_{mod}$') are compared with available experimental data and the results of DFT calculations and MD simulations employing different EAM-type potentials.

The values calculated with the original Gupta potential are consistent with some experimental and theoretical values reported in literature [22, 23, 52, 55, 57], whereas other works predicted either smaller or much larger values of E_{vf}. Note that the theoretical results reported in literature were obtained with different EAM-type potentials (Finnis − Sinclair and Gupta potentials as well as a distinct potential introduced in Ref. [54]) as well as with different EAM and modified EAM (MEAM) potentials. The variety of potentials and parameterizations used has resulted in a large (up to 40%) discrepancy between the calculated values of E_{vf}.

Calculations performed with the Gupta potential corrected by U_{lin} (see the column '$U_{Gup} + U_{lin}$') yield smaller values of E_{vf} as compared to the original Gupta potential, and the magnitude of the decrease depends on the parameter B. The values of E_{vf} listed in Table 3 were obtained for each metal using the B values that reproduce the

T a b l e 3

**Comparison of the vacancy formation energy E_{vf} obtained
in this paper with the published experimental and calculated data**

Element	Vacancy formation energy E_{vf}, eV					
	U_{Gup}	$U_{Gup} + U_{lin}$	$U_{Gup} + U_{mod}$	Experiment	Calculation	
					EAM-type	DFT
Ag	0.94	0.90	0.91	0.99 ± 0.06 [52] 1.09 ± 0.10 [53]	0.79 [19] (Gupta) 0.88 [22] (Gupta) 0.97 [23] (EAM) 1.10 [54]	–
Au	0.72	0.58	0.81	0.62 – 0.67 [55] 0.70 – 1.10 [55]	0.60 [19] (Gupta) 0.75 [22] (Gupta) 1.03 [23] (EAM) 1.10 [54]	–
Ti	1.49	1.22	1.44	1.55 [56]	1.43 [21] (FS) 1.49 [57] (EAM) 1.56 [58] (Gupta) 1.78 [59] (MEAM) 1.79 [28] (MEAM)	1.97 [60] 2.14 [61]

N o t a t i o n: U_{Gup} corresponds to the E_{vf} value calculated with the original EAM-type Gupta potential; ($U_{Gup} + U_{lin}$), ($U_{Gup} + U_{mod}$) correspond to the E_{vf} values done using the potential corrected by U_{lin} and the new modification U_{mod}; EAM, MEAM – embedded-atom method and modified EAM [51]; DFT is the density functional theory; FS is the Finnis – Sinclair potential [41].

experimental bulk melting temperatures (see Fig. 4). The figure shows that for $r_c \approx 8$ Å the value of B for silver, 0.0016 eV/Å, is three times smaller than that for gold, 0.005 eV/Å, and five times smaller than for titanium, 0.008 eV/Å. As a result, the vacancy-formation energy for silver calculated by means of the linear correction is slightly (by about 5%) smaller than the value predicted by the original Gupta potential. For gold and especially titanium, larger values of B should be used to reproduce the experimental bulk melting temperatures, which leads to a more pronounced decrease of E_{vf}. The magnitude of this discrepancy for titanium is within the uncertainty range of the existing theoretical data obtained by means of different EAM-type potentials (see Table 3). In MD simulations reported in literature [21, 28, 57−59] E_{vf} varies from about 1.4 to 1.8 eV while DFT calculations [60, 61] predicted even larger values up to 2.1 eV.

The sigmoid-type modification U_{mod} gives the results which are closer to the experimental values and the results of other MD simulations [21 − 23, 57] compared to the original Gupta potential and linear correction. This is due to the change

in the asymptotic behavior of the original Gupta potential, i.e., the weakening of interatomic interactions at large distances.

Table 4 presents the equilibrium lattice constants for silver, gold and titanium calculated with U_{Gup}, $U_{Gup} + U_{lin}$ and $U_{Gup} + U_{mod}$. The force created by the linear correction causes a uniform strain on crystals, which become uniformly compressed. For silver and gold this effect is rather small (the relative change in the lattice parameters is less than 1%) while the relative shortening of titanium crystals is about 2.5%. This can also be attributed to a very steep linear correction (i.e., a large force) that should be used to reproduce the experimental bulk melting temperature of Ti. Note also that the geometry optimization of a Ti crystal using the original Gupta potential yields the structure which is elongated along the [0001] axis as compared to the experimental value (the calculated lattice parameter $c = 4.75$ Å vs. the experimental value of 4.68 Å). The geometry optimization by means of the linear correction results in a uniform compression of the crystal, which brings the parameter c in a better agreement with the experimental value.
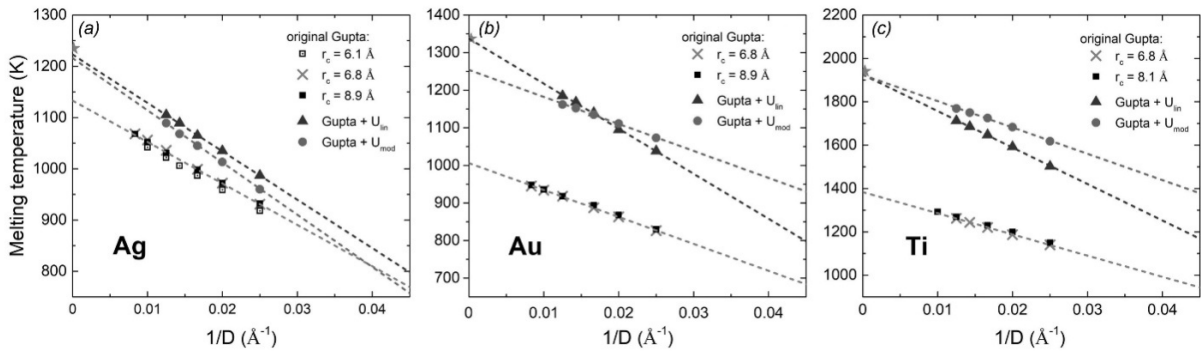
Fig. 5. Melting temperature of Ag (*a*), Au (*b*) and Ti (*c*) nanoparticles of diameter *D* calculated by 3 ways: using the original EAM-type Gupta potential (Eq. (2)), its linear correction U_{lin} (Eq. (3)) and the new modification U_{mod} (Eq. (7)); 3 values of r_c were considered (symbols). The extrapolation of the calculated numbers to the bulk limit was made (lines). Experimental values of bulk melting temperature are shown by stars

T a b l e 4

Comparison of the calculated equilibrium lattice constants with experimental data

Element	Equilibrium lattice constant, Å			
	U_{Gup}	$U_{Gup} + U_{lin}$	$U_{Gup} + U_{mod}$	Experiment [50]
Ag	4.07	4.05	4.07	4.09
Au	4.06	4.03	4.09	4.08
Ti (*a*)	2.91	2.83	2.89	2.95
Ti (*c*)	4.75	4.63	4.77	4.68

F o o t n o t e. The presented results were calculated with the original Gupta potential (U_{Gup}), as well as with the Gupta potential corrected by U_{lin} and the new modification U_{mod}. Two lattice parameters, *a* and *c*, are listed for titanium.

The sigmoid-type modification U_{mod} has a small impact on the equilibrium lattice parameters, which almost coincide with those predicted by the original Gupta potential and agree reasonably well with the experimental results. Contrary to the linear correction, U_{mod} does not induce a strong compression of the Ti crystal and its lattice parameters obtained by means of U_{mod} are similar to those calculated with U_{Gup}. As discussed above, this is due to the functional form of U_{mod} wherein a positive contribution of U'_{mod} plays the role at small interatomic distances (which span over a few nearest atomic layers) while a negative contribution of U'_{mod} plays the role at larger values of *r*.

Fig. 5 shows the melting temperatures of finite-sized Ag, Au and Ti nanoparticles as function of their inverse diameter, $1/D$. For all these metals, the bulk melting temperature predicted by the original Gupta potential is significantly lower than the experimental values. The most il-

lustrative example is titanium (see Fig. 5,*c*) whose melting temperature calculated with U_{Gup} is approximately 1380 K. It is more than 500 K lower than the experimental value of 1941 K (marked by a star symbol) which yields the relative discrepancy of about 30%. A similar feature has been observed for gold and silver — the absolute discrepancy is smaller for these metals (about 330 K and 100 K, respectively) while the relative discrepancy for gold is as large as 25%. These results further justify the necessity of correcting the EAM-type potential to bring the calculated bulk melting temperatures in closer agreement with the experimental values. The modification U_{mod} produces a similar effect as the linear correction — it leads to an increase in nanoparticles' melting temperatures and, as a result, to an increase in bulk melting temperatures. The new modification improves the calculated bulk melting temperature for the three metals considered. Good

agreement with the experimental values has been obtained for titanium and silver (the relative discrepancies from the experimental values are 0.8 and 1.5%, respectively) while a somewhat larger discrepancy of about 6% has been observed for gold. This is linked to the observation that the sigmoid-type modification increases the slope of the $T_m(1/D)$ dependence for silver and titanium nanoparticles but it almost does not change the slope for gold nanoparticles. The utilized parameters of U_{mod} for gold have been chosen such that all the quantities considered in this work agree better with experimental data as compared to the original Gupta potential. An even better agreement might be achieved by performing a more detailed analysis of the multidimensional parameter surface of U_{mod}. A finer tuning of parameters should bring the calculated T_m^{bulk} for gold to a better agreement with experimental data.

Summary

We formulated a recipe for modification of classical embedded-atom method (EAM)-type potentials aiming at a quantitative description of both equilibrium and nonequilibrium properties of metal systems by means of molecular dynamics simulations. The modification suggested in this work asymptotically approaches zero at large interatomic distances and generalizes the previously developed linear correction [38]. A general procedure for constructing the modified EAM-type potential was outlined and the relation between parameters of the new modification and the linear correction was elaborated.

The procedure developed has been applied to analyze the melting temperature as well as lattice constants, cohesive energy and vacancy formation energy of nanosystems made of silver, gold and titanium. It was demonstrated that the modified potential leads to an increase in the melting temperature of the metals and to a better agreement with experimental values as compared to the uncorrected EAM-type potential. The new modification induces a small (on the order of a few per cent or less) change of the equilibrium properties but increases the bulk melting temperature by more than 30% as it is demonstrated for the case of titanium. We have considered the many-body Gupta potential as an example but the generality of the correction allows its application in combination with other potentials of the EAM type such as Sutton − Chen or Finnis − Sinclair potentials. The results presented for the metals with cubic and hexagonal crystalline lattices further confirm a wide range of applicability of the proposed modification.

Appendix

Derivation of parameters of U_{mod}

To analytically derive the parameters of the sigmoid-type potential $U_{mod}(r)$, the latter was approximated by a piecewise linear function:

$$\bar{U}_{mod}(r) = \begin{cases} B_1 r + C_1, & r < R_0 \\ B_2 r + C_2, & R_0 < r < R_2 \\ 0, & r > R_2 \end{cases} \quad (8)$$

where $B_1 > 0$ ($C_1 < 0$) and $B_2 < 0$ ($C_2 > 0$),

$$R_0 = -\frac{C_1 - C_2}{B_1 - B_2}$$

is the point of intersection of the two linear segments, and $R_2 = -C_2/B_2$ is the point where $\bar{U}_{mod}(r) = 0$ (see dotted curves in Fig. 3). After substituting Eq. (8) into Eq. (4) and carrying out the integration one arrives at the condition:

$$\frac{(1-\gamma)^4}{(1-\beta)^3} = -\frac{\gamma^4}{\beta^3} \quad (9)$$

where $\beta = B_2/B_1$ and $\gamma = C_2/C_1$.

Substituting Eq. (8) in Eq. (6) one derives the force F_{mod} due to the potential $\bar{U}_{mod}(r)$. This force should be equal to the force F_{lin} arising due to the linear correction at a given cutoff in order to increase the melting temperature by the same value. This can be expressed as

$$\left(\frac{4}{3}\right)^3 \frac{C^3}{B^2} = \frac{C_1^3}{B_1^2}\left[\frac{(1-\gamma)^3}{(1-\beta)^2} + \frac{\gamma^3}{\beta^2}\right]. \quad (10)$$

The procedure for deriving the parameters of the sigmoid-type function U_{mod} (7) and its approximation $\bar{U}_{mod}$ (8) can be summarized as follows:

(*i*) The parameters B and C of the linear correction are obtained as described in the section 'Linear correction to EAM-type potentials';

(*ii*) Fixing the point $R_1 = -C_1/B_1$ at which $U_{mod}(r) = 0$ (see Fig. 3) a scan over different values of B_1 and C_1 is performed;

(*iii*) β and γ are derived from the numerical solution of Eqs. (9) and (10), and the corresponding values of B_2 and C_2 are obtained;

(*iv*) Repeating steps (*i*) − (*iii*) for different combinations (B_1, C_1) one obtains a multidimensional parameter surface (B_1, C_1, B_2, C_2);

(*v*) Once $B_{1,2}$, $C_{1,2}$ are derived, the resulting piecewise function is fitted with the sigmoid-type function U_{mod}, Eq. (7), to obtain the parameters λ and r_s.

Acknowledgments

REFERENCES

1. **Andreoni W., Yip S.** (Eds.), Handbook of materials modeling. Methods: theory and modeling, 2nd ed., Springer International Publishing, Cham, 2019.

2. **Rapaport D.C.,** The art of molecular dynamics simulation, 2nd ed., Cambridge University Press, 2011.

3. **Solov'yov I.A., Korol A.V., Solov'yov A.V.,** Multiscale modeling of complex molecular structure and dynamics with MBN Explorer, Springer International Publishing, Cham, 2017.

4. **Hoyt J.J., Asta M., Sadigh B.,** Test of the universal scaling law for the diffusion coeffcient in liquid metals, Phys. Rev. Lett. 85 (3) (2000) 594−597.

5. **Sushko G.B., Verkhovtsev A.V., Yakubovich A.V., et al.,** Molecular dynamics simulation of self-diffusion processes in titanium in bulk material on grain junctions and on surface, J. Phys. Chem. A. 118 (33) (2014) 6685−6691.

6. **Cheng B., Paxton A.T., Ceriotti M.,** Hydrogen diffusion and trapping in α-iron: the role of quantum and anharmonic fluctuations, Phys. Rev. Lett. 120 (22) (2018) 225901.

7. **Verkhovtsev A.V., Yakubovich A.V., Sushko G.B., et al.,** Molecular dynamics simulations of the nanoindentation process of titanium crystal, Comput. Mater. Sci. 76 (August) (2013) 20−26.

8. **Zink M., Samwer K., Johnson W.L., Mayr S.G.,** Plastic deformation of metallic glasses: size of shear transformation zones from molecular dynamics simulations, Phys. Rev. B. 73 (17) (2006) 172203.

9. **Cleveland C.L., Luedtke W.D., Landman U.,** Melting of gold clusters: icosahedral precursors, Phys. Rev. Lett. 81 (10) (1998) 2036−2039.

10. **Qi Y., Cagin T., Johnson W.L., Goddard III W.A.,** Melting and crystallization in Ni nanoclusters: the mesoscale regime, J. Chem. Phys. 115 (1) (2001) 385−394.

11. **Lyalin A., Hussien A., Solov'yov A.V., Greiner W.,** Impurity effects on the melting of Ni clusters, Phys. Rev. B. 79 (16) (2009) 165403.

12. **Yakubovich A.V., Sushko G.B., Schramm S., Solov'yov A.V.,** Kinetics of liquid-solid phase transition in large nickel clusters, Phys. Rev. B. 88 (3) (2013) 035438.

13. **Purja Pun G.P., Mishin Y.,** Molecular dynamics simulation of the martensitic phase transformation in NiAl alloys, J. Phys.: Condens. Matter 22 (29) (2010) 295403.

14. **Kexel C., Schramm S., Solov'yov A.V.,** Atomistic simulation of martensite-austenite phase transition in nanoscale nickel-titanium crystals, Eur. Phys. J. B. 88 (9) (2015) 221.

15. **Kim S.-G., Horstemeyer M.F., Baskes M.I., et al.,** Semi-empirical potential methods for atomistic simulations of metals and their construction procedures, J. Eng. Mater. Technol. 131 (4) (2009) 041210.

16. **Lloyd J.R., Luo T.** (Eds.), Handbook of molecular dynamics potential functions, Begell

House, New York, Connecticut, 2011.

17. **Müser M.H.,** Semi-empirical interatomic potentials: recent advances and challenges, Modelling Simul. Mater. Sci. Eng. 23 (7) (2015) 070401.

18. **Rassoulinejad-Mousavi S.M., Zhang Y.,** Interatomic potentials transferability for molecular simulations: a comparative study for platinum, gold and silver, Sci. Rep. 8 (2018) 2424.

19. **Rosato V., Guellope M., Legrand B.,** Thermodynamical and structural properties of f.c.c. transition metals using a simple tight-binding model, Philos. Mag. A. 59 (2) (1989) 321−326.

20. **Sutton A.P., Chen J.,** Long-range Finnis − Sinclair potentials, Philos. Mag. Lett. 61 (3) (1990) 139−146.

21. **Ackland G.J.,** Theoretical study of titanium surfaces and defects with a new many-body potential, Philos. Mag. A. 66 (6) (1992) 917−932.

22. **Cleri F., Rosato V.,** Tight-binding potentials for transition metals and alloys, Phys. Rev. B. 48 (1) (1993) 22−33.

23. **Foiles S.M., Baskes M.I., Daw M.S.,** Embedded-atom-method functions for the fcc metals Cu, Ag, Au, Ni, Pd, Pt, and their alloys, Phys. Rev. B. 33 (12) (1986) 7983−7991.

24. **Daw M.S., Foiles S.M., Baskes M.I.,** The embedded-atom method: a review of theory and applications, Mater. Sci. Rep. 9 (7−8) (1993) 251−310.

25. **Mishin Y., Asta M., Li J.,** Atomistic modeling of interfaces and their impact on microstructure and properties, Acta Mater. 58 (4) (2010) 1117−1151.

26. **Lang L., Yang K., Tian Z., et al.,** Development of a Ni-Mo interatomic potential for irradiation simulation, Modelling Simul. Mater. Sci. Eng. 27 (4) (2019) 045009.

27. **Kavousi S., Novak B.R., Baskes M.I., et al.,** Modified embedded-atom method potential for high-temperature crystal-melt properties of Ti-Ni alloys and its application to phase field simulation of solidification, Modelling Simul. Mater. Sci. Eng. 28 (1) (2020) 015006.

28. **Kim Y.-M., Lee B.-J., Baskes M.I.,** Modified embedded-atom method interatomic potentials for Ti and Zr, Phys. Rev. B. 74 (1) (2006) 014101.

29. **Ryu S., Weinberger C.R., Baskes M.I., Cai W.,** Improved modified embedded-atom method potentials for gold and silicon, Modelling Simul. Mater. Sci. Eng. 17 (7) (2009) 075008.

30. **Lewis L.J., Jensen P., Barrat J.-L.,** Melting, freezing, and coalescence of gold nanoclusters, Phys. Rev. B. 56 (4) (1997) 2248−2257.

31. **Nordlund K., Kuronen A.,** Non-equilibrium properties of GaAs interatomic potentials, Nucl. Instrum. Meth. B. 159 (3) (1999) 183−186.

32. **Wang Z.W., Palmer R.E.,** Determination of the ground-state atomic structures of size-selected Au nanoclusters by electron-beam-induced transformation, Phys. Rev. Lett. 108 (24) (2012) 245502.

33. **Sushko G.B., Solov'yov I.A., Solov'yov A.V.,** Molecular dynamics for irradiation driven chemistry: application to the FEBID process, Eur. Phys. J. D. 70(10) (2016) 217.

34. **Huth M., Porrati F., Schwalb C., et al.,** Focused electron beam induced deposition: a perspective, Beilstein J. Nanotechnol. 3 (2012) 597−619.

35. **Sturgeon J.B., Laird B.B.,** Adjusting the melting point of a model system via Gibbs-Duhem integration: application to a model of aluminum, Phys. Rev. B. 62 (22) (2000) 14720−14727.

36. **Ackland G.J.,** Temperature dependence in interatomic potentials and an improved potential for Ti, J. Phys.: Conf. Ser. 402 (2012) 012001.

37. **Mendelev M.I., Underwood T.L., Ackland G.J.,** Development of an interatomic potential for the simulation of defects, plasticity and phase transformations in titanium, J. Chem. Phys. 145 (15) (2016) 154102.

38. **Sushko G.B., Verkhovtsev A.V., Kexel C., et al.,** Reconciling simulated melting and ground-state properties of metals with a modified embedded-atom method potential, J. Phys.: Condens. Matter. 28 (14) (2016) 145201.

39. **Gupta R.P.** Lattice relaxation at a metal surface, Phys. Rev. B. 23 (12) (1981) 6265−6270.

40. **Kexel C., Verkhovtsev A.V., Sushko G.B., et al.,** Toward the exploration of the NiTi phase diagram with a classical force field, J. Phys. Chem. C. 120 (43) (2016) 25043−25052.

41. **Finnis M.W., Sinclair J.E.,** A simple empirical N-body potential for transition metals, Philos. Mag. A. 50 (1) (1984) 45−55.

42. **Ackland G.J., Finnis M.W., Vitek V.,**

Validity of the second moment tight-binding model, J. Phys. F: Met. Phys. 18 (8) (1988) L153−L157.

43. **Goringe C.M., Bowler D.R., Hernandez E.,** Tight-binding modelling of materials, Rep. Prog. Phys. 60 (12) (1997) 1447−1512.

44. **Daw M.S., Baskes M.I.,** Semiempirical, quantum mechanical calculation of hydrogen embrittlement in metals, Phys. Rev. Lett. 50 (17) (1983) 1285−1288.

45. **Dzugutov M.,** Glass formation in a simple monatomic liquid with icosahedral inherent local order, Phys. Rev. A. 46 (6) (1992) 2984−2987.

46. **Solov'yov I.A., Yakubovich A.V., Nikolaev P.V., et al.,** MBN Explorer − a universal program for multiscale computer simulations of complex molecular structure and dynamics, J. Comput. Chem. 33 (30) (2012) 2412−2439.

47. **Sushko G.B., Solov'yov I.A., Solov'yov A.V.,** Modeling MesoBioNano systems with MBN Studio made easy, J. Mol. Graph. Model. 88 (May) (2019) 247−260.

48. **Pawlow P.,** Über die Abhängigkeit des Schmelzpunktes von der Oberflächenenergie eines festen Körpers, Z. Phys. Chem. 65 (1909) 1−35.

49. **Calvo F.,** Thermodynamics of nanoalloys, Phys. Chem. Chem. Phys. 17 (42) (2015) 27922−27939.

50. **Kittel C.,** Introduction to Solid State Physics, 7th ed., Wiley, 1995.

51. **Baskes M.I.,** Modified embedded-atom potentials for cubic materials and impurities, Phys. Rev. B. 46 (5) (1992) 2727−2742.

52. **McGervey J.D., Triftshäuser W.,** Vacancy-formation energies in copper and silver from positron annihilation, Phys. Lett. A. 44 (1) (1973) 53−54.

53. **Simmons R.O., Balluffi R.W.,** Measurement of the equilibrium concentration of lattice vacancies in silver near the melting point, Phys. Rev. 119 (2) (1960) 600−605.

54. **Doyama M., Kogure Y.,** Embedded atom potentials in fcc metals, Radiat. Eff. Defects Solids. 142 (1−4) (1997) 107−114.

55. **Jongenburger P.,** Energy of formation of vacancies in copper and gold, Phys. Rev. 106 (1) (1957) 66−69.

56. **Shestopal V.O.,** Specific heat and vacancy formation in titanium at high temperatures, Sov. Phys. Solid State. 7 (11) (1966) 2798−2799.

57. **Johnson R.A.,** Many-body effects on calculated defect properties in h.c.p. metals, Philos. Mag. A 63 (5) (1991) 865−872.

58. **Lai W.S., Liu B.X.,** Lattice stability of some Ni−Ti alloy phases versus their chemical composition and disordering, J. Phys.: Condens. Matter 12 (5) (2000) L53−L60.

59. **Baskes M.I., Johnson R.A.,** Modified embedded atom potentials for HCP metals, Modelling Simul. Mater. Sci. Eng. 2 (1) (1994) 147−163.

60. **Raji A.T., Scandolo S., Mazzarello R., et al.,** Ab initio pseudopotential study of vacancies and self-interstitials in HCP titanium, Philos. Mag. 89 (20) (2009) 1629−1645.

61. **Le Bacq O., Willaime F., Pasturel A.,** Unrelaxed vacancy formation energies in group-IV elements calculated by the full-potential linear Muffin-tin orbital method: invariance with crystal structure, Phys. Rev. B. 59 (13) (1999) 8508−8515.

62. **Korzhavyi P.A., Abrikosov I.A., Johansson B., et al.,** First-principles calculations of the vacancy formation energy in transition and noble metals, Phys. Rev. B. 59 (18) (1999) 11693−11703.

63. **Mattsson T.R., Mattsson A.E.,** Calculating the vacancy formation energy in metals: Pt, Pd, and Mo, Phys. Rev. B. 66 (21) (2002) 214110.

THE AUTHORS

VERKHOVTSEV Alexey V.

MBN Research Center at Frankfurt Innovation Center of Biotechnology

3 Altenhöferallee, Frankfurt am Main, 60438, Germany

verkhovtsev@mbnexplorer.com

KOROL Andrei V.
MBN Research Center at Frankfurt Innovation Center of Biotechnology
3 Altenhöferallee, Frankfurt am Main, 60438, Germany
korol@mbnexplorer.com

SUSHKO Gennady B.
MBN Research Center at Frankfurt Innovation Center of Biotechnology
3 Altenhöferallee, Frankfurt am Main,60438, Germany
sushko@mbnexplorer.com

SCHRAMM Stefan
Goethe University Frankfurt
1 Max-von-Laue St., Frankfurt am Main, 60438, Germany

SOLOV'YOV Andrey V.
MBN Research Center at Frankfurt Innovation Center of Biotechnology
3 Altenhöferallee, Frankfurt am Main, 60438, Germany
solovyov@mbnresearch.com

СПИСОК ЛИТЕРАТУРЫ

1. **Andreoni W., Yip S.** (Eds.). Handbook of materials modeling. Methods: theory and modeling. 2nd Ed. Springer International Publishing, Cham. 2019. 1987 p.

2. **Rapaport D.C.** The art of molecular dynamics simulation. 2nd Ed. Cambridge: Cambridge University Press, 2011. 549 p.

3. **Solov'yov I.A., Korol A.V., Solov'yov A.V.** Multiscale modeling of complex molecular structure and dynamics with MBN Explorer. Springer International Publishing, Cham. 2017. 451 p.

4. **Hoyt J.J., Asta M., Sadigh B.** Test of the universal scaling law for the diffusion coeffcient in liquid metals // Phys. Rev. Lett. 2000. Vol. 85. No. 3. Pp. 594−597.

5. **Sushko G.B., Verkhovtsev A.V., Yakubovich A.V., Schramm S., Solov'yov A.V.** Molecular dynamics simulation of self-diffusion processes in titanium in bulk material, on grain junctions and on surface // J. Phys. Chem. A. 2014. Vol. 118. No. 33. Pp. 6685−6691.

6. **Cheng B., Paxton A.T., Ceriotti M.** Hydrogen diffusion and trapping in α-iron: the role of quantum and anharmonic fluctuations // Phys. Rev. Lett. 2018. Vol. 120. No. 22. P. 225901.

7. **Verkhovtsev A.V., Yakubovich A.V., Sushko G.B., Hanauske M., Solov'yov A.V.** Molecular dynamics simulations of the nanoindentation process of titanium crystal // Comput. Mater. Sci. 2013. Vol. 76. August. Pp. 20−26.

8. **Zink M., Samwer K., Johnson W.L., Mayr S.G.** Plastic deformation of metallic glasses: size of shear transformation zones from molecular dynamics simulations // Phys. Rev. B. 2006. Vol. 73. No. 17. P. 172203.

9. **Cleveland C.L., Luedtke W.D., Landman U.** Melting of gold clusters: icosahedral precursors // Phys. Rev. Lett. 1998. Vol. 81. No. 10. Pp. 2036−2039.

10. **Qi Y., Cagin T., Johnson W.L., Goddard III W.A.** Melting and crystallization in Ni nanoclusters: the mesoscale regime // J. Chem. Phys. 2001. Vol. 115. No. 1. Pp. 385−394.

11. **Lyalin A., Hussien A., Solov'yov A.V., Greiner W.** Impurity effects on the melting of Ni clusters // Phys. Rev. B. 2009. Vol. 79. No. 16. P. 165403.

12. **Yakubovich A.V., Sushko G.B., Schramm S., Solov'yov A.V.** Kinetics of liquid-solid phase transition in large nickel clusters // Phys. Rev. B. 2013. Vol. 88. No. 3. P. 035438.

13. **Purja Pun G.P., Mishin Y.** Molecular dynamics simulation of the martensitic phase transformation in NiAl alloys // J. Phys.: Condens. Matter. 2010. Vol. 22. No. 29. P. 295403.

14. **Kexel C., Schramm S., Solov'yov A.V.**

Atomistic simulation of martensite-austenite phase transition in nanoscale nickel-titanium crystals // Eur. Phys. J. B. 2015. Vol. 88. No. 9. P. 221.

15. **Kim S.-G., Horstemeyer M.F., Baskes M.I., Rais-Rohani M., Kim S., Jelinek B., Houze J., Moitra A., Liyanage L.** Semi-empirical potential methods for atomistic simulations of metals and their construction procedures // J. Eng. Mater. Technol. 2009. Vol. 131. No. 4. P. 041210.

16. **Lloyd J.R., Luo T.** (Eds.). Handbook of molecular dynamics potential functions. New York, Connecticut: Begell House, 2011. 245 p.

17. **Müser M.H.** Semi-empirical interatomic potentials: recent advances and challenges // Modelling Simul. Mater. Sci. Eng. 2015. Vol. 23. No. 7. P. 070401.

18. **Rassoulinejad-Mousavi S.M., Zhang Y.** Interatomic potentials transferability for molecular simulations: a comparative study for platinum, gold and silver // Sci. Rep. 2018. Vol. 8. P. 2424.

19. **Rosato V., Guellope M., Legrand B.** Thermodynamical and structural properties of f.c.c. transition metals using a simple tight-binding model // Philos. Mag. A. 1989. Vol. 59. No. 2. Pp. 321−326.

20. **Sutton A.P., Chen J.** Long-range Finnis − Sinclair potentials // Philos. Mag. Lett. 1990. Vol. 61. No. 3. Pp. 139−146.

21. **Ackland G.J.** Theoretical study of titanium surfaces and defects with a new many-body potential // Philos. Mag. A. 1992. Vol. 66. No. 6. Pp. 917−932.

22. **Cleri F., Rosato V.** Tight-binding potentials for transition metals and alloys // Phys. Rev. B. 1993. Vol. 48. No. 1. Pp. 22−33.

23. **Foiles S.M., Baskes M.I., Daw M.S.** Embedded-atom-method functions for the fcc metals Cu, Ag, Au, Ni, Pd, Pt, and their alloys // Phys. Rev. B. 1986. Vol. 33. No. 12. Pp. 7983−7991.

24. **Daw M.S., Foiles S.M., Baskes M.I.** The embedded-atom method: a review of theory and applications // Mater. Sci. Rep. 1993. Vol. 9. No. 7−8. Pp. 251−310.

25. **Mishin Y., Asta M., Li J.** Atomistic modeling of interfaces and their impact on microstructure and properties // Acta Mater. 2010. Vol. 58. No. 4. Pp. 1117−1151.

26. **Lang L., Yang K., Tian Z., Deng H., Gao F., Hu W., Mo Y.** Development of a Ni-Mo interatomic potential for irradiation simulation // Modelling Simul. Mater. Sci. Eng. 2019. Vol. 27. No. 4. P. 045009.

27. **Kavousi S., Novak B.R., Baskes M.I., Asle Zaeem M., Moldovan D.** Modified embedded-atom method potential for high-temperature crystal-melt properties of Ti-Ni alloys and its application to phase field simulation of solidification // Modelling Simul. Mater. Sci. Eng. 2020. Vol. 28. No. 1. P. 015006.

28. **Kim Y.-M., Lee B.-J., Baskes M.I.** Modified embedded-atom method interatomic potentials for Ti and Zr // Phys. Rev. B. 2006. Vol. 74. No. 1. P. 014101.

29. **Ryu S., Weinberger C.R., Baskes M.I., Cai W.** Improved modified embedded-atom method potentials for gold and silicon // Modelling Simul. Mater. Sci. Eng. 2009. Vol. 17. No. 7. P. 075008.

30. **Lewis L.J., Jensen P., Barrat J.-L.** Melting, freezing, and coalescence of gold nanoclusters // Phys. Rev. B. 1997. Vol. 56. No. 4. Pp. 2248−2257.

31. **Nordlund K., Kuronen A.** Non-equilibrium properties of GaAs interatomic potentials // Nucl. Instrum. Meth. B. 1999. Vol. 159. No. 3. Pp. 183−186.

32. **Wang Z.W., Palmer R.E.** Determination of the ground-state atomic structures of size-selected Au nanoclusters by electron-beam-induced transformation // Phys. Rev. Lett. 2012. Vol. 108. No. 24. P. 245502.

33. **Sushko G.B., Solov'yov I.A., Solov'yov A.V.** Molecular dynamics for irradiation driven chemistry: application to the FEBID process // Eur. Phys. J. D. 2016. Vol. 70. No. 10. P. 217.

34. **Huth M., Porrati F., Schwalb C., Winhold M., Sachser R., Dukic M., Adams J., Fantner G.** Focused electron beam induced deposition: a perspective // Beilstein J. Nanotechnol. 2012. Vol. 3. Pp. 597−619.

35. **Sturgeon J.B., Laird B.B.** Adjusting the melting point of a model system via Gibbs-Duhem integration: application to a model of aluminum // Phys. Rev. B. 2000. Vol. 62. No. 22. Pp. 14720−14727.

36. **Ackland G.J.** Temperature dependence in interatomic potentials and an improved poten-

tial for Ti // J. Phys.: Conf. Ser. 2012. Vol. 402. P. 012001

37. **Mendelev M.I., Underwood T.L., Ackland G.J.** Development of an interatomic potential for the simulation of defects, plasticity and phase transformations in titanium // J. Chem. Phys. 2016. Vol. 145. No. 15. P. 154102.

38. **Sushko G.B., Verkhovtsev A.V., Kexel C., Korol A.V., Schramm S., Solov'yov A.V.** Reconciling simulated melting and ground-state properties of metals with a modified embedded-atom method potential // J. Phys.: Condens. Matter. 2016. Vol. 28. No. 14. P. 145201.

39. **Gupta R.P.** Lattice relaxation at a metal surface // Phys. Rev. B. 1981. Vol. 23. No. 12. Pp. 6265–6270.

40. **Kexel C., Verkhovtsev A.V., Sushko G.B., Korol A.V., Schramm S., Solov'yov A.V.** Toward the exploration of the NiTi phase diagram with a classical force field // J. Phys. Chem. C. 2016. Vol. 120. No. 43. Pp. 25043–25052.

41. **Finnis M.W., Sinclair J.E.** A simple empirical N-body potential for transition metals // Philos. Mag. A. 1984. Vol. 50. No. 1. Pp. 45–55.

42. **Ackland G.J., Finnis M.W., Vitek V.** Validity of the second moment tight-binding model // J. Phys. F: Met. Phys. 1988. Vol. 18. No. 8. Pp. L153–L157.

43. **Goringe C.M., Bowler D.R., Hernandez E.** Tight-binding modelling of materials // Rep. Prog. Phys. 1997. Vol. 60. No. 12. Pp. 1447–1512.

44. **Daw M.S., Baskes M.I.** Semiempirical, quantum mechanical calculation of hydrogen embrittlement in metals // Phys. Rev. Lett. 1983. Vol. 50. No. 17. Pp. 1285–1288.

45. **Dzugutov M.** Glass formation in a simple monatomic liquid with icosahedral inherent local order // Phys. Rev. A. 1992. Vol. 46. No. 6. Pp. 2984–2987.

46. **Solov'yov I.A., Yakubovich A.V., Nikolaev P.V., Volkovets I., Solov'yov A.V.** MBN Explorer – a universal program for multiscale computer simulations of complex molecular structure and dynamics // J. Comput. Chem. 2012. Vol. 33. No. 30. Pp. 2412–2439.

47. **Sushko G.B., Solov'yov I.A., Solov'yov A.V.** Modeling MesoBioNano systems with MBN Studio made easy // J. Mol. Graph. Model. 2019.

Vol. 88. May. Pp. 247–260.

48. **Pawlow P.** Über die Abhängigkeit des Schmelzpunktes von der Oberflächenenergie eines festen Körpers // Z. Phys. Chem. 1909. Vol. 65. Pp. 1–35.

49. **Calvo F.** Thermodynamics of nanoalloys // Phys. Chem. Chem. Phys. 2015. Vol. 17. No. 42. Pp. 27922–27939.

50. **Киттель Ч.** Введение в физику твердого тела. М.: Наука, 1978. 791 с.

51. **Baskes M.I.** Modified embedded-atom potentials for cubic materials and impurities // Phys. Rev. B. 1992. Vol.46. No. 5. Pp. 2727–2742.

52. **McGervey J.D., Triftshäuser W.** Vacancy-formation energies in copper and silver from positron annihilation // Phys. Lett. A. 1973. Vol. 44. No. 1. Pp. 53–54.

53. **Simmons R.O., Balluffi R.W.** Measurement of the equilibrium concentration of lattice vacancies in silver near the melting point // Phys. Rev. 1960. Vol. 119. No. 2. Pp. 600–605.

54. **Doyama M., Kogure Y.** Embedded atom potentials in fcc metals // Radiat. Eff. Defects Solids. 1997. Vol. 142. No. 1–4. Pp. 107–114.

55. **Jongenburger P.** Energy of formation of vacancies in copper and gold // Phys. Rev. 1957. Vol. 106. No. 1. Pp. 66–69.

56. **Шестопал В.О.** Теплоемкость и образование вакансий в титане при высоких температурах // Физика твердого тела. 1965. Т. 7. Вып. 11. С. 3461–3462.

57. **Johnson R.A.** Many-body effects on calculated defect properties in h.c.p. metals // Philos. Mag. A. 1991. Vol. 63. No. 5. Pp. 865–872.

58. **Lai W.S., Liu B.X.** Lattice stability of some Ni–Ti alloy phases versus their chemical composition and disordering // J. Phys.: Condens. Matter. 2000. Vol. 12. No. 5. Pp. L53–L60.

59. **Baskes M.I., Johnson R.A.** Modified embedded atom potentials for HCP metals // Modelling Simul. Mater. Sci. Eng. 1994. Vol. 2. No. 1. Pp. 147–163.

60. **Raji A.T., Scandolo S., Mazzarello R., Nsengiyumva S., Härting M., Britton D.T.** Ab initio pseudopotential study of vacancies and self-interstitials in HCP titanium // Philos. Mag. 2009. Vol. 89. No. 20. Pp. 1629–1645.

61. **Le Bacq O., Willaime F., Pasturel A.** Un-

relaxed vacancy formation energies in group-IV elements calculated by the full-potential linear Muffin-tin orbital method: invariance with crystal structure // Phys. Rev. B. 1999. Vol. 59. No. 13. Pp. 8508−8515.

62. **Korzhavyi P.A., Abrikosov I.A., Johansson B., Ruban A.V., Skriver H.L.** First-principles cal-culations of the vacancy formation energy in transi-tion and noble metals // Phys. Rev. B. 1999. Vol. 59. No. 18. Pp. 11693−11703.

63. **Mattsson T.R., Mattsson A.E.** Calculat-ing the vacancy formation energy in metals: Pt, Pd, and Mo // Phys. Rev. B. 2002. Vol. 66. No. 21. P. 214110.

СВЕДЕНИЯ ОБ АВТОРАХ

ВЕРХОВЦЕВ Алексей Валерьевич — *Ph.D., научный сотрудник Научно-исследовательского центра мезобионаносистем (MBN), г. Франкфурт-на-Майне, Германия.*
60438, Германия, г. Франкфурт-на-Майне, Альтенхёфераллее, 3
verkhovtsev@mbnexplorer.com

КОРОЛЬ Андрей Владимирович — *кандидат физико-математических наук, доцент, научный сотрудник Научно-исследовательского центра мезобионаносистем (MBN), г. Франкфурт-на-Майне, Германия.*
60438, Германия, г. Франкфурт-на-Майне, Альтенхёфераллее, 3
korol@mbnexplorer.com

СУШКО Геннадий Борисович — *Ph.D., научный сотрудник Научно-исследовательского центра мезобионаносистем (MBN), г. Франкфурт-на-Майне, Германия.*
60438, Германия, Франкфурт-на-Майне, Альтенхёфераллее, 3
sushko@mbnexplorer.com

ШРАММ Штефан — *Ph.D., профессор Центра научных вычислений Франкфуртского университета им. Гёте.*
60438, Германия, Франкфурт-на-Майне, Макс-фон-Лауэ штрассе, 1

СОЛОВЬЁВ Андрей Владимирович — *доктор физико-математических наук, профессор Научно-исследовательского центра мезобионаносистем (MBN), г. Франкфурт-на-Майне, Германия.*
60438, Германия, г. Франкфурт-на-Майне, Альтенхёфераллее, 3
solovyov@mbnresearch.com